ASTRONOMY AND ASTROPHYSICS LIBRARY

Joachim E. Trümper
Günther Hasinger (Eds.)

The Universe in X-Rays

With 237 Figures, 40 in Color and 19 Tables

Springer

Joachim E. Trümper
Günther Hasinger

Max-Planck-Institut
für extraterrestische Physik
Giessenbachstraße
85748 Garching
Germany
E-mail: jtrumper@mpe.mpg.de
grh@mpe.mpg.de

Cover illustrations: above: ROSAT all-sky survey; from Max-Planck-Institut fuer extraterrestrische Physik; below: 15. Nov. 2006, Credit: NASA/CXC/MIT/UMass Amherst/M.D. Stage et al.

Library of Congress Control Number: 2007933496

ISSN 0941-7834
ISBN 978-3-540-34411-7 Springer Berlin Heidelberg New York

Springer is a part of Springer Science+Business Media
springer.com

Typesetting by SPi using a Springer LATEX macro package

Cover design: eStudio Calamar, Girona/Spain

Printed on acid-free paper SPIN: 11328858 55/SPi 5 4 3 2 1 0

Preface

In the early years of X-ray astronomy, one of us (J. E. T.) had always a book in reach, entitled "X-ray Astronomy" and edited by Riccardo Giacconi and Herbert Gursky about a decade after they had opened the field by the discovery of Scorpius X-1 and the X-ray background. This book summarized all the knowledge at the time, based on the results from the pioneering rocket and balloon experiments and from Uhuru, the first satellite entirely dedicated to X-ray astronomy.

Since those early times X-ray astronomy has evolved with enormous pace. The number of known sources has increased by a factor of thousand, but more important, they now comprise almost all classes of astronomical objects – from planets, moons and comets out to clusters of galaxies and quasars. In the era of multi-wavelength astronomy X-ray observations provide insight into extreme physical conditions prevailing in all these sources – very high temperatures, very strong gravitational fields, super-nuclear densities, extreme concentrations of relativistic particles.

The intent of this book is to summarize the present status of the field, which has become quite challenging, since the number of publications in refereed journals has risen to more than 20 000. Therefore the coverage cannot be complete, but must rather be representative. We apologize for omitting any important ideas, methods or results.

The authors of the various chapters are mainly scientists working at the Max-Planck-Institute for Extraterrestrial Physics, the home of ROSAT, or colleagues who have been working closely with us during the last 20 years. Besides ROSAT, the main sources of information have been the other X-ray satellites of the nineties – ASCA, RXTE and BeppoSAX – and their more recent successors – Chandra, XMM-Newton, INTEGRAL, Swift and Suzaku – which have used novel instrumentation to produce a wealth of knowledge on the universe seen at high energies.

This book addresses mainly scientists who are teaching the subject, and young scientists entering the field, as well as astronomers from neighbouring disciplines and physicists interested in one of the most exciting fields of astrophysics. It is organized in a straightforward way: We start with a discussion of instruments and methods in part I and then continue in parts II and III with the status of galactic and extragalactic X-ray astronomy respectively, ordering the contributions in a geocentric fashion. In Chapter 26 a short summary of the current plans for future missions in X-ray astronomy is given.

We are very thankful to all authors of this book for their contributions. The editorial assistance of Konrad Dennerl who brought the LaTeX manuscript into its final shape is gratefully acknowledged. We thank Birgit Boller and Walburga Frankenhuizen for their dedicated secretarial support, as well as Maria Fürmetz and Barbara Mory for their painstaking work on the index of the book.

Garching, November 2007

Joachim E. Trümper
Günther Hasinger

Contents

Part II Galactic X-Ray Astronomy

List of Contributors

Werner Becker
Max-Planck-Institut für extraterrestrische Physik, Giessenbachstraße,
85748 Garching, Germany
e-mail: web@mpe.mpg.de

Klaus Beuermann
Institut für Astrophysik, Friedrich-Hund-Platz 1, 37077 Göttingen, Germany,
e-mail: beuermann@astro.physik. uni-goettingen.de

Hans Böhringer
Max-Planck-Institut für extraterrestrische Physik, Giessenbachstraße,
85748 Garching, Germany
e-mail: hxb@mpe.mpg.de

Thomas Boller
Max-Planck-Institut für extraterrestrische Physik, Giessenbachstraße,
85748 Garching, Germany
e-mail: bol@mpe.mpg.de

Dieter Breitschwerdt
Universität Wien, Türkenschanzstraße 17, 1180 Wien, Austria,
e-mail: breitschwerdt@univie.ac.at

Konrad Dennerl
Max-Planck-Institut für extraterrestrische Physik, Giessenbachstraße,
85748 Garching, Germany
e-mail: kod@mpe.mpg.de

Michael Freyberg
Max-Planck-Institut für extraterrestrische Physik, Giessenbachstraße,
85748 Garching, Germany
e-mail: mjf@mpe.mpg.de

Peter Friedrich
Max-Planck-Institut für extraterrestrische Physik, Giessenbachstraße,
85748 Garching, Germany
e-mail: pfriedrich@mpe.mpg.de

Jochen Greiner
Max-Planck-Institut für extraterrestrische Physik, Giessenbachstraße,
85748 Garching, Germany
e-mail: jcg@mpe.mpg.de

Frank Haberl
Max-Planck-Institut für extraterrestrische Physik, Giessenbachstraße,
85748 Garching, Germany
e-mail: fwh@mpe.mpg.de

Günther Hasinger
Max-Planck-Institut für extraterrestrische Physik, Giessenbachstraße,
85748 Garching, Germany
e-mail: ghasinger@mpe.mpg.de

Eckhard Kendziorra
Institut für Astronomie und Astrophysik, Universität Tübingen, Sand 1,
72076 Tübingen, Germany
e-mail: kendziorra@astro.uni-tuebingen.de

Stefanie Komossa
Max-Planck-Institut für extraterrestrische Physik, Giessenbachstraße,
85748 Garching, Germany
e-mail: skomossa@mpe.mpg.de

Joachim Krautter
Landessternwarte, Königstuhl, 69117 Heidelberg, Germany
e-mail: jkrautte@lsw-uni-heidelberg.de

Norbert Meidinger
Max-Planck-Institut für extraterrestrische Physik, Giessenbachstraße,
85748 Garching; MPI Halbleiterlabor, Otto-Hahn-Ring 6, 81739 München,
Germany
e-mail: nom@hll.mpg.de

Robert Petre
X-ray Astrophysics Laboratory, NASA / Goddard Space Flight Center,
Greenbelt, MD 20771, USA,
e-mail: robert.petre-1@nasa.gov

Wolfgang Pietsch
Max-Planck-Institut für extraterrestrische Physik, Giessenbachstraße,
85748 Garching, Germany
e-mail: wnp@mpe.mpg.de

Elmar Pfeffermann
Max-Planck-Institut für extraterrestrische Physik, Giessenbachstraße,
85748 Garching, Germany
e-mail: epf@mpe.mpg.de

Peter Predehl
Max-Planck-Institut für extraterrestrische Physik, Giessenbachstraße,
85748 Garching, Germany
e-mail: predehl@mpe.mpg.de

Jürgen H.M.M. Schmitt
Hamburger Sternwarte, Gojenbergsweg 11, 21029 Hamburg, Germany
e-mail: jschmitt@hs.uni-hamburg.de

Rüdiger Staubert
Institut für Astronomie und Astrophysik, Univ. Tübingen, Sand 1, 72076 Tübingen, Germany
e-mail: staubert@astro. uni-tuebingen.de

Beate Stelzer
Osservatorio Astronomico di Palermo, Piazza del Parlamento 1, 90134 Palermo, Italien,
e-mail: stelzer@astropa.unipa.it

Lothar Strüder
Max-Planck-Institut für extraterrestrische Physik, Giessenbachstraße,
85748 Garching; MPI Halbleiterlabor, Otto-Hahn-Ring 6, 81739 München, Germany
e-mail: lts@hll.mpg.de

Yasuo Tanaka
Max-Planck-Institut für extraterrestrische Physik, Giessenbachstraße,
85748 Garching, Germany
e-mail: ytanaka@mpe.mpg.de

Joachim Trümper
Max-Planck-Institut für extraterrestrische Physik, Giessenbachstraße,
85748 Garching, Germany
e-mail: jtrumper@mpe.mpg.de

Klaus Werner
Institut für Astronomie und Astrophysik, Universität Tübingen, Sand 1,
72076 Tübingen, Germany
e-mail: werner@astro.uni-tuebingen.de

Part I

X-Ray Astronomical Instrumentation

1 Overview

R. Staubert and J. Trümper

The advancement of X-ray astronomy since its start about half a century ago has been strongly dependent on the development of instruments and observational techniques. Since the earth's atmosphere is opaque for X- and gamma-rays this field could only develop in parallel to space technology providing the necessary carriers, which can place X-ray astronomy telescopes and detectors near or beyond the boundaries of our atmosphere. In the early days, in the sixties and seventies, stratospheric balloons and rockets played an important role, albeit with severe limitations on altitude ($\sim$40 km, leaving still substantial absorption) and on observing time of a few minutes, respectively. Today, satellites are available allowing X-ray astronomy missions to last for a decade or longer. The principle mode of measurement in X-ray astronomy is to detect individual photons with the aim to determine the complete set of four properties: arrival direction (leading to images), the energy and the time of arrival of the photon, and its polarization angle. The first detectors were proportional counters and scintillation counters, originally developed for detecting charged particles in nuclear physics research. They had effective areas of a few hundred square centimeters and were usually equipped with mechanical collimators providing some indirect imaging capability through the restriction of the field of view (typically to a few square degrees) and the possibility for scanning observations. An important challenge for these detectors was the reduction of the background radiation, both from photons of the diffuse X-ray sky background and from charged particles of the ever present cosmic rays. This was achieved by narrow colimators and the invention of various techniques of anticoincidence and veto schemes, as perfected for example in multiwire proportional counters. The first X-ray satellite Uhuru, launched in December 1970, carried collimated gas proportional counters and was scanning the entire X-ray sky. The detection of $\sim$400 X-ray sources marked a quantum leap in X-ray astronomy. The so called "gas scintillation proportional counter," combined the two physical detector principles and gave an improved energy resolution, but had limited application and scientific impact.

The next major step was the introduction of focusing and imaging X-ray optics, the Wolter telescope, together with imaging detectors in the focal plane providing two-dimensional X-ray images. The first satellite mission, the Einstein Observatory, carrying such a telescope with the imaging proportional counter (IPC) and the high resolution imager (HRI) as focal plane detectors allowed a break through in two areas: extended objects could directly be imaged, and for all sources the sensitivity

J.E. Trümper and G. Hasinger (eds.), *The Universe in X-Rays.*

was greatly improved through the focusing and the corresponding background reduction.

ROSAT performed the first all sky survey with an imaging telescope. Using a greatly improved telescope and detector technology, it provided a large step in the observational capabilities, both in the number of detected X-ray sources ($\sim$125.000), and through the large number of pointings throughout the remaining 8 years of the mission. Today the standard focal plane detector is based on actively cooled pixelized solid state detectors (CCDs), which provide a higher energy resolution and wider energy range than proportional counters. The use of CCDs was pioneered by ASCA and further perfected on Chandra and XMM-Newton.

In parallel to imaging telescopes, high resolution grating spectrometers were developed, first used in the Einstein Observatory and today with great success in the Chandra and XMM-Newton missions. Intensive work has also gone into the development of very deeply cooled bolometers, which have a great potential because of their very high spectral resolution and large throughput. Unfortunately, the first bolometer flown on a satellite exploded with ASTRO-E, and the second attempt on Suzaku failed because the cryogenic coolant was lost before the observations commenced. At higher photon energies ($>$10 keV), focusing becomes difficult and the current technique is imaging by spatial aperture modulation, the so called "coded mask" technique, first used in the Mir-KVANT mission and now on INTEGRAL. Efforts are underway to develop also focusing telescopes for hard X-rays and even gamma-rays by employing multilayer-coded reflecting surfaces or making use of Bragg reflection on crystals. Polarimetry is still in a rudimentary state. Imaging, high resolution spectroscopy, and high time resolution measurements have reached a high level of sophistication with a corresponding wealth of scientific results, but there is still a wide open field for further advances.

2 Proportional Counters

E. Pfeffermann

2.1 Introduction

After the discovery of the first extra-solar X-ray source in 1962 with a gaseous detector, the proportional counter became the workhorse instrument of soft X-ray astronomy for nearly four decades. The origin of gaseous detectors dates back to the early twentieth century, when Rutherford and Geiger published in 1908: "An electrical method of counting the number of α-particles from radioactive substances" [23]. Cosmic rays were discovered in 1912 with a gaseous detector by V. Hess. During the first half of the twentieth century much progress was made in the technology of gaseous detectors in the fields of nuclear and cosmic-ray physics [8]. For instance, the discovery of the effect of quench gases allowed a stable operation of gas detectors [28]. Ionization-dependent output signals of gas counters were observed first by Geiger and Klemperer [7]. About 10 years later, proportional counters were developed [13]. First attempts to operate multiwire detectors were carried out in conjunction with the Manhatten project [22]. In 1968, Charpak and collaborators succeeded in the development and operation of multiwire proportional counters (MWPC) [4]. These detectors combine the advantages of a large sensitive area with multidimensional event parameter sensing. Many innovative ideas arose from the group around Charpak. The development of gaseous detectors is still going on. New detector types like the micro strip gas chamber (MSGC) [15] and micro pattern gas detectors (MPGD) like the gas electron multiplier (GEM) have been described [25].

2.2 Gaseous Detectors

A gaseous detector is basically a capacitor filled with gas. Electrons and ions generated by ionizing radiation in the gas are collected by the corresponding electrodes. The acceleration of the charges in the electrical field extracts energy from the capacitor. Therefore, the electrodes show signals before the charges arrive at the electrodes. Depending on the gas and the electrical field strength in the capacitor, the instrument operates in different modes. At moderate electrical field strengths, electrons and ions are just collected by the electrodes, this is the so called ionization-chamber mode. At a higher field strength, the electrons gain enough energy on a mean free path

J.E. Trümper and G. Hasinger (eds.), *The Universe in X-Rays.*

length to excite the gas atoms (in this case a pure noble gas) resulting in the emission of UV light. The detector operates as a gas scintillation proportional counter. A further increase of the electrical field enables the electrons to ionize gas atoms by collisions and charge multiplication takes place. As long as the charge generated by the multiplication process is proportional to the original number of electrons, the detector is in the proportional counter mode. At higher electrical fields the detector enters the Geiger mode, where the avalanche propagates through the whole detector. The saturated signals are no longer proportional to the original charge. The spark chamber mode is the subsequent mode at the highest field strength. The ionizing event triggers a spark discharge of the counter. It depends on the skill of the detector designer that the instrument stays in the desired operating conditions even in the harsh space environment.

2.3 Operation Principle of a Proportional Counter

The simplest geometry of a proportional counter is a gas-filled cylindrical conductive tube with a coaxial thin wire as shown in Fig. 2.1. The wire is connected to a positive high voltage and coupled via a capacitor to a charge sensitive preamplifier. For the detection of X-rays, the cathode tube has to have a window, transparent to the required energy band. X-rays entering the detector volume through the window interact with the detector gas. At X-ray energies up to 50 keV the predominant interaction process is the photo effect. The photo effect cross section scales as $Z^n E^{-\frac{8}{3}}$, where E is the X-ray energy and Z is the atomic number of the detector gas and $n \approx 4$–5. The number N of electron–ion pairs generated by this event can be written as $N = E/W$, where E is the energy of the absorbed X-ray photon and W the average energy for the creation of one electron–ion pair in the detector gas (usually a noble gas with an additive of a molecular gas like CO_2 or CH_4). The average energy for the creation of an electron–ion pair depends on the detector gas and is about 25–30 eV. A 1 keV X-ray photon creates 30–40 electron–ion pairs. Electrons and ions drift in the electrical field of the detector to the anode wire and the cathode, respectively. If the electrons gain enough energy over a mean free path length to ionize the detector gas, charge multiplication takes place. The actual charge reduplicates on average after each ionizing collision of the electrons. This happens in the vicinity

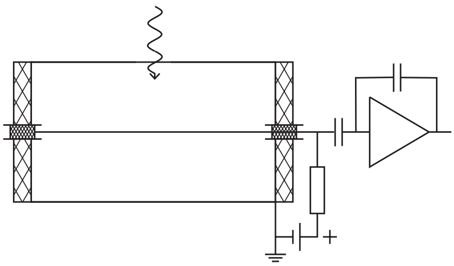

Fig. 2.1 Single wire proportional counter

of the anode wire, where the electrical field is in the order of $10^5\,\mathrm{V\,cm^{-1}}$. In this cylindrical geometry, the electrical field strength as a function of the radial distance r from the tube center is: $\mathrm{d}U/\mathrm{d}r = U_\mathrm{o}/[r(\ln r_\mathrm{c}/r_\mathrm{a})]$ with U_o = anode wire voltage, r_a = anode wire radius, r_c = cathode tube radius . The movement of electrons and ions extracts energy from the electrical field generating displacement currents on anode and cathode. The electrons move about three orders of magnitude faster than the ions and the majority of the charge is generated only several mean free path lengths away from the anode wire. Therefore, the waveform of the output signal of the detector has a small fraction with a short rise time, contributed by the electrons. The main portion of the signal, with a rise time of 100 µs or more, is generated by the movement of the ions. Not only charge multiplication takes place in the avalanche, but also the generation of UV photons both by excitation of gas atoms and by the neutralization of positive ions on arrival at the cathode. UV photons hitting the cathode induce the emission of electrons from cathode surface, when the work function of the cathode material is less than the photon energy. These electrons in turn can cause subsequent avalanches possibly leading to a permanent discharge of the counter. The addition of several % of a polyatomic gas (quench gas) to the detector gas prevents this problem. Quench gases absorb UV photons emitted by the noble gas and convert them via radiationless transitions finally into heat. Via charge exchange quench gases reduce also the number of noble gas ions arriving at the cathode. Quench gases can speed up the drift velocity of electrons quite dramatically reducing the influence of gas impurities [24].

2.3.1 Quantum Efficiency of Proportional Counters

The quantum efficiency of a proportional counter for X-rays is determined by the transmission of the window and the absorption of the detector gas. To achieve a high transmission rather thin windows are used. A thin window has to be supported by a grid to withstand the gas pressure. The X-ray transmission of the support structure is usually energy independent and reduces the transmission by a constant factor (T). Proportional counters with a permanent gas filling have to use metallic window materials like beryllium or aluminum. Metallic window materials limit the detectable X-ray band to energies above 1.5 keV. Detectors using plastic window materials like polypropylene (about 1 µm thick) are able to detect X-ray photons down to 0.1 keV. Because of the gas diffusion through the plastic window such detectors have to use a gas supply system. Figure 2.2 shows the X-ray transmission of a 1 µm polypropylene foil and a 25 µm beryllium foil as a function of energy. The absorption of X-rays in the detector gas, usually a mixture of a noble gas with 5–20% quench gas, depends on the atomic numbers of the gas mixture, the gas pressure, and the dimension of the absorption region. For low energies, the basic constituent of the gas mixture is argon, whereas for higher energies increasing admixtures of xenon or pure xenon with a quench gas is used. The quantum efficiency of the detector can be written:

$$Q = Te^{-d\mu_\mathrm{w}}(1 - e^{-g\mu_\mathrm{g}}) \tag{2.1}$$

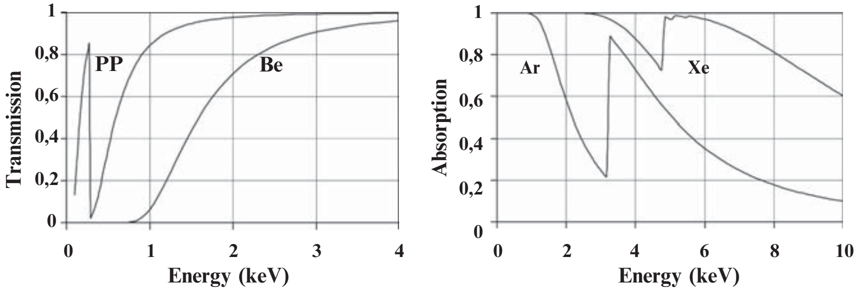

Fig. 2.2 *Left panel* shows the transmission of two window materials 25 μm beryllium (Be) and 1 μm polypropylene (PP). The *right panel* shows the absorption of 1 cm of argon (Ar) and xenon (Xe) at a pressure of 1 bar as a function of X-ray energy [10]

d and g are the window and gas column densities in g cm^{-2}. μ_w, μ_g are the corresponding energy-dependent mass absorption coefficients.

2.3.2 Energy Resolution

Proportional counters have a moderate energy resolution. The energy resolution is mainly determined by the statistics of the initial ionization process and the statistics of charge multiplication. The variation of the number N of electron–ion pairs created by the ionizing event is less than that estimated from Poisson statistics, because the collisions of the ionization process are not statistically independent. The Fano factor F is an empirical constant to adapt the experimental observed variance to the predicted one [5].

$$\left(\frac{\sigma_N}{N}\right)^2 = \frac{F}{N}; \qquad F \approx 0.05 - 0.2 \tag{2.2}$$

For large values of multiplication, the variance of the amplification A of a single electron is [12]:

$$\left(\frac{\sigma_A}{\bar{A}}\right)^2 \simeq b; \qquad b \approx 0.5 - 0.6 \tag{2.3}$$

Therefore, the energy resolution of a proportional counter is:

$$\left(\frac{\sigma_E}{E}\right)^2 = \left(\frac{\sigma_N}{N}\right)^2 + \frac{1}{N}\left(\frac{\sigma_A}{\bar{A}}\right)^2 \tag{2.4}$$

$$\frac{\sigma_E}{E} = \sqrt{\frac{F+b}{N}} = \sqrt{\frac{W(F+b)}{E}} \tag{2.5}$$

These estimates give a limit for the best achievable energy resolution. Gas impurities, tolerances of anode wire diameter, and loss of electrons at the entrance window can deteriorate the energy resolution of the proportional counter.

2.3.3 Time Resolution

Because of the high drift velocity of electrons in gases (10^6–10^7 cm s^{-1} at moderate electrical fields, see for instance [24]), proportional counters have a good time resolution. In cylindrical geometry, only the electron drift time between the absorption position of the X-ray photon and the avalanche region contributes substantially to the time uncertainty. Depending on detector geometry time resolution below 1µs can be achieved.

2.3.4 Background Rejection Capability

Detectors for X-ray astronomy operated in space are exposed to the whole spectrum of cosmic rays. The background rate exceeds by far the X-ray event rate of the majority of cosmic X-ray sources. A sophisticated event selection logic is mandatory to distinguish real X-ray events from charged particle events or fluorescent X-rays from surrounding materials. One possibility is to limit the energy band of accepted events. The depth of the detector cell must be chosen large enough so that minimum ionizing particles deposit more energy than the most energetic accepted X-ray event. In this way, minimum ionizing particles can be easily discriminated with an upper event threshold. Another possibility to distinguish particle events from X-ray events is the geometric shape of the related ionization cloud. Particle events leave an ionized track, whereas X-ray events leave a more point-like ionization cloud resulting in different rise times of the detector signal. A further background reduction method is to surround the actual X-ray detector with anticoincidence detectors on three to five sides. Coincident signals in an anticoincidence counter and the X-ray detector indicate with a high probability a non X-ray interaction and the event should be rejected. To eliminate X-rays generated by cosmic rays in the detector housing, the gas column density of the anticoincidence counter should be large enough to absorb X-rays efficiently up to the upper threshold of the accepted energy band. Large area X-ray detectors achieve by these methods background rejection efficiencies of 99.6% [6].

2.3.5 Detector Lifetime

The lifetime of detectors in the harsh space environment is a major concern to the involved experimenters. The radiation environment can damage a proportional counter in two ways. Heavy ionizing particles can deposit energies 3–4 orders of magnitude higher than X-rays within the nominal operating range. These huge amount of charges must not trigger a permanent discharge or destroy the detector by spark discharge. In low earth orbit (ROSAT orbit at 580 km), heavy ionizing events have a trigger rate of about 2×10^{-4} cm^{-2} s^{-1} behind 1.5 cm of aluminum.

Gas detectors suffer a permanent aging because of the cracking of the quench gas molecules during normal operation. Hydrocarbons like CH_4 tend to deposit polymerization products on anode and cathode wires, resulting in gain shifts and or permanent discharge (Malter effect) of the detector after accumulation of a not very well-defined critical charge per millimeter of anode wire. Many parameters like gas purity, gas composition, wire, housing and sealing materials, and last but not least the electrical field contribute to the radiation dose tolerated by the detector [19]. Sealed detectors tolerate a charge dose of 10^{-5} C mm^{-1} anode wire for an Ar–CH_4 gas filling but only 10^{-7} C mm^{-1} for a Xe–CH_4 gas before serious degradation occurs [26]. Therefore, many large area proportional counters for X-ray astronomy use CO_2 as quench gas. CO_2 does not polymerize. Only carbon deposits have been observed [21].

2.4 Large Area Proportional Counters for X-Ray Astronomy

The observation of the weak photon fluxes from cosmic X-ray sources with non-imaging instruments (detectors with mechanical collimators) requires large area detectors with high background rejection capability. Table 2.1 shows the development of collecting area of several proportional counter experiments for X-ray astronomy within the last decades. Multi anode multilayer proportional counters subdivided in cells by cathode grids as shown in Fig. 2.3 were mainly used for such observations in the energy band up to 50 keV. The cell structure of these detectors offers different possibilities for discriminating background events. Using the signals of the detector cells bordering the walls of the detector housing in anticoincidence results in a three-sided anticoincidence. Additional end-veto electrodes of anode or cathode protect the other two sides of the sensitive volume [3, 30]. Requiring that a single event must not show signals in neighboring cells reduces charged particle background from the front side. The loss of real X-ray events, because of photoelectron tracks crossing the border of two cells, is less than 10% in the 1.5–35 keV band [6]. Another approach was used in the RXTE detector by introducing a separate front anticoincidence layer filled with a low Z gas (propane) separated from the lower detector volume by an aluminized mylar foil [2].

Table 2.1 Several large area proportional counters for X-ray astronomy

Experiment	Year	ΔE (ke V)	Area (cm^2)	FOV (FWHM)	Reference
Uhuru	1970	2.0–20	2×840	$5° \times 5°, 5° \times 0.5°$	[9]
HEAO-1 A1	1977	0.15–20	7×1350–1900	$1° \times 4° - 1° \times 0.5°$	[18]
EXOSAT ME	1983	1.2–50	1800	$0.75° \times 0.75°$	[29]
Ginga LAC	1987	1.5–37	4000	$1.1° \times 2°$ elliptical	[30]
RXTE PCA	1995	2.0–60	6250	1° hexagonal	[2]

Collimator field of view (FOV)

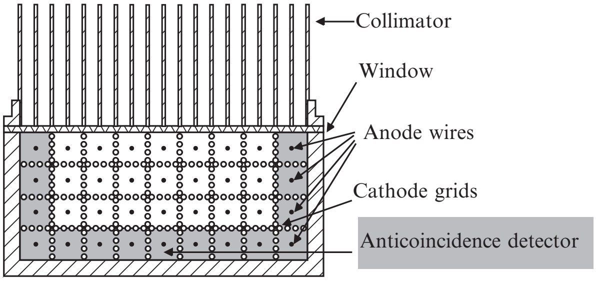

Fig. 2.3 Large area proportional counter for X-ray astronomy

The detection limit of such an instrument for a point source in the presence of a diffuse X-ray background component and a cosmic-ray background can be estimated as follows if the observed quantities are constant.

Q = quantum efficiency of the detector
A_x = geometric detector area for X-rays (cm^2)
A_b = geometric detector area for background (cm^2)
B_c = cosmic-ray background events not rejected by event selection logic (events $cm^{-2}\,s^{-1}\,keV^{-1}$)
B_x = diffuse cosmic X-rays background (events $cm^{-2}\,s^{-1}\,keV^{-1}\,sr^{-1}$)
Ω = field of view in (sr)
F_{min} = minimum detectable flux of a point source (Photons $cm^{-2}\,s^{-1}\,keV^{-1}$)
ΔE = energy band of detector (keV)
S = desired number of standard deviations
t = observing time (s)

$$F_{min} = \frac{S}{QA_x}\sqrt{\frac{B_c A_b + Q\Omega B_x A_x}{t\Delta E}} \tag{2.6}$$

2.5 Gas Scintillation Proportional Counters

Gas scintillation proportional counters (GSPC), developed in 1972 [20], offer the advantage of an enhanced energy resolution when compared with proportional counters. In conventional proportional counters, the charge generated by an ionizing event is multiplied in a high electrical field. The amplification grows exponentially with the number of ionizing collisions of an electron in the high field region. Only 14 ionizing collisions result in a charge multiplication of four orders of magnitude. The variation in the number of ionizing collisions during multiplication degrades the Fano limited energy resolution of proportional counters by almost a factor of two (see Chap. 2.3.2 energy resolution). In gas scintillation proportional counters (see Fig. 2.4), the charge released by an ionizing event is not amplified. Similar to multiwire proportional counters, X-rays are absorbed by the detector gas (usually a

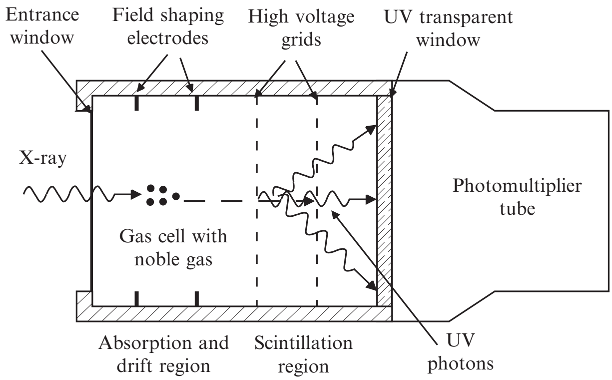

Fig. 2.4 Gas scintillation proportional counter

noble gas or a mixture of noble gases) in an absorption and drift region. The electrons drift from this low field region into the high field scintillation region where they acquire sufficient energy to excite the scintillation of the detector gas, but not to ionize it. In case of xenon, diatomic molecules, formed by the collision of excited atoms, deexcite by the emission of UV photons in the wavelength band of 150–195 nm [14]. The number of scintillation photons increase linearly with the number of exciting collisions of the electrons with the gas atoms. These collisions are independent events. Therefore, the variation of the light output generated during the scintillation process depends on the statistics of the final number of photons registered by the photomultiplier. The integral intensity of the light flash is proportional to the energy of the ionizing event. GSPCs can reach an energy resolution nearly at the Fano limit because of the large amount of scintillation photons.

GSPCs are rather intolerant to gas impurities because of the low electron mobility in xenon. Therefore, the gas cell of GSPCs has to be manufactured with ultra-high vacuum technology to avoid contamination of the detector gas. In addition, gas purification systems like getter pumps are used. The slow velocity of the electrons in the absorption and drift region with a low electrical field strength intensifies the susceptibility of the GSPC to gas impurities. This effect can be reduced in the so called "driftless" GSPC. The "driftless" GSPC has a common high field absorption–scintillation region located directly below the detector window. The high electrical field mandatory for the scintillation excitation of the gas by the electrons results in a high drift velocity of the electrons from the beginning. The high field reduces in addition the loss of electrons from the ionization cloud of X-ray events absorbed near to the entrance window. But nothing is for free and the light output of an event in this configuration depends on the absorption depth of the X-ray event in the absorption–scintillation region. To recover the original energy of the event, the signal has to be corrected with a burst length factor.

X-ray astronomy with nonimaging detectors requires large apertures and a good background rejection efficiency. Rise time discrimination, burst length discrimination, and limitation of the energy band are the main background suppression

Table 2.2 Characteristics of GSPC instruments for X-ray astronomy

Satellite	BeppoSAX	EXOSAT	Tenma
Year	1996	1983	1983
Experiment	HPGSPC	GS	SPC-A, SPC-B, SPC-C
Effective area	$240\,cm^2$ *	$\sim 100\,cm^2$	$320\ cm^2$, $320\ cm^2$, $80\ cm^2$
FOV (FWHM)	1.1°	0.75°	3.1°, 2.5°, 3.8° mod. collimator
Energy range	4–120 keV	2–40 keV	2–60 keV
$\Delta E/E$ (% FWHM)	$31 \times (E(keV))^{-0.5}$	$27 \times (E(keV))^{-0.5}$	$23 \times (E(keV))^{-0.5}$
Reference	[1]	[16, 17]	[27]

* @ 30 keV

methods for GSPCs to distinguish background events from real X-ray signals. The background rejection efficiency by the burst length discrimination can be improved substantially by using a gas mixture of xenon with helium. Addition of helium increases the electron drift velocity considerably compared with pure xenon [11]. The full field energy resolution of large area GSPCs with a single photomultiplier readout is degraded because of solid angle variations of the light emission regions for events distributed over the whole sensitive area. A focusing electrical field in a conical absorption and drift region concentrating the electrons on a small scintillation region reduce the effect of solid angle variation. Large aperture detectors with such focusing geometries were operated on the X-ray satellites Tenma and EXOSAT [11, 16]. Another approach to overcome the problem of solid angle variations in large area detectors is to view the scintillation region of the GSPC by an Anger camera arrangement of several photomultipliers. The event position derived from the ratio of the photomultiplier signals is used to correct the event energy. This method was used in the HPGSPC experiment aboard BeppoSAX. Table 2.2 gives the characteristics of GSPCs with mechanical collimators operated on several X-ray astronomy satellite missions.

References

1. Boella, G., Butler, R. C., Perola, G. C., et al. 1997, Astron. Astrophys. Suppl., 122, 299
2. Bradt, H. V., Rothschild, R. E. and Swank, J. H. 1993, Astron. Astrophys. Suppl., 97, 355
3. Brunner, A. N., Kraushaar, W. L., McCammon, D., et al. 1973, Rev. Sci. Instrum., 44, 418
4. Charpak, G., Bouclier, R., Bressani, T., et al. 1968, Nucl. Instr. Meth., 62, 235
5. Fano, U. 1947, Phys. Rev., 72, 26
6. Fraser, G.W. 1989, X-Ray Detectors in Astronomy, Cambridge University Press, Cambridge, pp 35–95
7. Geiger, H., Klemperer, O. 1928, Z. Phys., 49, 753
8. Geiger, H., Müller, W. 1928, Phys. Z., 29, 839
9. Giacconi, R., Kellogg, E., Gorenstein, P., et al. 1971, Astrophys. J., 165, L27
10. Henke, B. L., Gullikson, E. M., Davis, J. C. 1993, Atomic Data and Nuclear Data Tables, 54(2), 181